JOURNAL OF GEOPHYSICAL RESEARCH, VOL. 106, NO. A6, PAGES 10,691–10,704, JUNE 1, 2001

Two-dimensional global hybrid simulation of pressure evolution and waves in the magnetosheath

Y. Lin,[1] R. E. Denton,[2] L. C. Lee,[3] and J. K. Chao[4]

Abstract. A two-dimensional hybrid simulation is carried out for the global structure of the magnetosheath. Quasi-perpendicular magnetosonic/fast mode waves with large-amplitude in-phase oscillations of the magnetic field and the ion density are seen near the bow shock transition. Alfvén/ion-cyclotron waves are observed along the streamlines in the magnetosheath, and the wave power peaks in the middle magnetosheath. Antiphase oscillations in the magnetic field and density are present away from the shock transition. Transport ratio analysis suggests that these oscillations result from mirror mode waves. Since fluid simulations are currently best able to model the global magnetosphere and the pressure in the magnetosphere is inherently anisotropic (parallel pressure $p_{\|} \neq$ perpendicular pressure $p_{\perp}$), it is of some interest to see if a fluid model can be used to predict the anisotropic pressure evolution of a plasma. Here the predictions of double adiabatic theory, the bounded anisotropy model, and the double polytropic model are tested using the two-dimensional hybrid simulation of the magnetosheath. Inputs to the models from the hybrid simulation are the initial post bow shock pressures and the time-dependent density and magnetic field strength along streamlines of the plasma. The success of the models is evaluated on the basis of how well they predict the subsequent evolution of $p_{\|}$ and $p_{\perp}$. The bounded anisotropy model, which encorporates a bound on $p_{\perp}/p_{\|}$ due to the effect of ion cyclotron pitch angle scattering, does a very good job of predicting the evolution of $p_{\perp}$; this is evidence that local transfer of energy due to waves is occurring. Further evidence is the positive identification of ion-cyclotron waves in the simulation. The lack of such a good prediction for the evolution of $p_{\|}$ appears to be due to the model's lack of time dependence for the wave-particle interaction and its neglect of the parallel heat flux. Estimates indicate that these effects will be less significant in the real magnetosheath, though perhaps not negligible.

1. Introduction

The magnetosheath is the plasma region downstream of the bow shock and surrounding the magnetosphere [*Kaufmann et al.*, 1970; *Fairfield*, 1971]. It consists of heated solar wind plasma that is slowed down and flows with the magnetic field, which drapes around the magnetosphere. Early magnetohydrodynamic (MHD) models of the magnetosheath can be traced back to *Midgley and Davis* [1963] and *Lees* [1964], who predicted a depletion of plasma density just outside of the magnetopause due to compression of the draped field lines against the dayside magnetopause. The depletion layer was further studied in detail by *Zwan and Wolf* [1976]. The evidence of this predicted plasma depletion layer was first reported by *Paschmann et al.* [1978] and *Crooker et al.* [1979].

Low-frequency waves in the magnetosheath have been frequently observed at the bow shock and in the magnetosheath; among them are mirror mode waves [*Tsurutani et al.*, 1982; *Hubert et al.*, 1989; *Lacombe et al.*, 1992; *Denton et al.*, 1995a; *Lin et al.*, 1998] and ion-cyclotron-like fluctuations [*Sckopke et al.*, 1990; *Anderson et al.*, 1991; *Farris et al.*, 1993]. Mirror waves are characterized by spatial fluctuations of wavelength greater than the ion gyroradius. They possess an antiphase relationship between the magnetic field strength B and the plasma density n. The thresholds of both the mirror wave and the ion-cyclotron wave instabilities require $T_{\perp}/T_{\|} > 1$ [e.g., *Hasegawa*, 1975; *Gary et al.*,

[1]Physics Department, Auburn University, Auburn, Alabama.

[2]Physics and Astronomy Department, Dartmouth College, Hanover, New Hampshire.

[3]Physics Department, National Cheng Kung University, Tainan, Taiwan.

[4]Institute of Space Science, National Central University, Chungli, Taiwan.

Paper number 2000JA000232.
0148-0227/01/2000JA000232$09.00

1994], where $T_\parallel$ and $T_\perp$ are the parallel and perpendicular ion temperatures, respectively. Satellite observations at quasi-perpendicular shocks, in which the angle between the interplanetary magnetic field (IMF) and the shock normal is greater than 45°, often show that ions have a sharp peak in $T_\perp/T_\parallel$ just downstream of the shock, which is caused by ion reflections at the bow shock [e.g., *Sckopke et al.*, 1983]. The high $T_\perp/T_\parallel$ distributions are believed to be the source that drives mirror and ion-cyclotron instabilities [*Winske and Quest*, 1988]. Immediately downstream of the bow shock, observations also show that the mirror instability is likely to produce magnetic fluctuations in the high β plasma [*Hubert et al.*, 1989] and that the ion-cyclotron anisotropy instability produces the strongest magnetic fluctuations in plasma regions with lower β.

Crooker and Siscoe [1977] suggested that magnetosheath flows may lead to

$$\beta_\perp/\beta_\parallel >> 1 + 1/\beta_\perp, \tag{1}$$

where $\beta_\parallel = 2\mu_0 p_\parallel/B^2$ and $\beta_\perp = 2\mu_0 p_\perp/B^2$ are the parallel and perpendicular ion β, respectively, with $p_\parallel$ being the ion pressure parallel to the magnetic field and $p_\perp$ being the perpendicular ion pressure. Since the cross section of a magnetic flux tube decreases as it convects to the subsolar magnetopause and the length of the flux tube increases, the double adiabatic equations [*Chew et al.*, 1956] imply that the transverse compression increases $T_\perp$ and that the longitudinal expansion decreases $T_\parallel$, indicating a condition in favor of mirror instability throughout the magnetosheath. *Price et al.* [1986] and *Lee et al.* [1988] carried out one-dimensional (1-D) hybrid simulations, in which ions are treated as individual particles and electrons are treated as a massless fluid, to show the existence of mirror mode instability under large $T_\perp/T_\parallel$ in the magnetosheath. Simulations and observations showed that the most unstable mirror waves propagate at angles between 50° and 80° relative to the magnetic field [e.g., *Tsurutani et al.*, 1982; *Price et al.*, 1986]. Nevertheless, the studies by *Price et al.* [1986] and *Gary* [1992] also indicate that the ion-cyclotron instability would tend to dominate the mirror instability by growing faster and suppressing the anisotropy. On the other hand, the 1-D hybrid simulation by *McKean et al.* [1992] suggested that an external compression of magnetic flux tubes, which may be caused by draping and compression of field lines in the magnetosheath, can maintain the anisotropy and thus enhance the mirror waves. The ion-cyclotron mode instability has also been simulated by *Gary et al.* [1996] using a two-dimensional (2-D) hybrid model of quasi-perpendicular shocks.

In this paper we present a global hybrid simulation of the magnetosheath. The evolution of the parallel and perpendicular pressures and the plasma kinetic instabilities in the magnetosheath are simulated using a 2-D model in which the bow shock, which contains both the quasi-parallel and the quasi-perpendicular parts along its curved front, and the magnetosheath are formed self-consistently by the supersonic solar wind passing the magnetosphere obstacle. As an introduction, the development of the models for the evolution of anisotropic pressure in the magnetosheath is given below.

In the double adiabatic theory of *Chew et al.* [1956], in which the heat flux is neglected, the second moment of the Boltzmann equation leads to the double adiabatic equations for the low-frequency evolution (frequency $\omega \ll$ the proton gyrofrequency Ω_p) of parallel ion pressure $p_\parallel$ and perpendicular ion pressure $p_\perp$,

$$\frac{d}{dt}\left(\frac{p_\perp}{nB}\right) = 0, \tag{2a}$$

$$\frac{d}{dt}\left(\frac{p_\parallel B^2}{n^3}\right) = 0, \tag{2b}$$

where the convective derivative $d/dt = (\partial/\partial t) + \mathbf{V}\cdot\nabla$, with $\mathbf{V}$ as the plasma velocity. Equations (2a) and (2b) assume that there is no coupling between parallel and perpendicular degrees of freedom.

The derivation of (2) does not include the effect of high-frequency waves in collisionless plasmas. Ion-cyclotron waves (with frequency close to the proton gyrofrequency) lead to a local exchange of energy which prevents the pressure anisotropy from exceeding a bound [*Denton et al.*, 1994, 1995b; *Gary et al.*, 1994], which can be expressed approximately [*Anderson et al.*, 1994] as

$$\left(\frac{p_\perp}{p_\parallel}\right)_{\text{And}} = 1 + 0.85\,\beta_\parallel^{-0.5}. \tag{3}$$

A similar bound has been reported by *Fuselier et al.* [1994] and *Phan et al.* [1994] from satellite observations and by *Gary et al.* [1996] from hybrid simulations of quasi-perpendicular shocks. The bounded anisotropy model [*Denton et al.*, 1994, 1995b] is a method of evolving $p_\parallel$ and $p_\perp$ which incorporates the effect of the ion-cyclotron waves. At each simulation time step, (2) is used to evolve $p_\parallel$ and $p_\perp$. If $p_\perp/p_\parallel$ exceeds $(p_\perp/p_\parallel)_{\text{And}}$ in (3), an exchange of energy is made from $p_\perp$ to $p_\parallel$ (keeping the total internal energy constant) so that $p_\perp/p_\parallel$ is reduced to $(p_\perp/p_\parallel)_{\text{And}}$. The bounded anisotropy model also assumes that the heat flux may be neglected.

The bounded anisotropy model was tested using magnetosheath data for time periods in which the observing spacecraft was relatively close to the subsolar line [*Denton et al.*, 1994, 1995b]. The results of these studies indicated that the model could do a good job of representing the separate evolution of $p_\perp$ and $p_\parallel$ in the magnetosheath. The bounded anisotropy model was also incorporated in various MHD models of the dayside magnetosheath flow [*Erkaev et al.*, 1999; *Samsonov and Pudovkin*, 2000]. In the fluid model of *Pudovkin et al.* [1999] the effects of a finite temperature anisotropy relaxation time were considered in the proton pitch angle diffusion during the energy exchange from $p_\perp$ to $p_\parallel$.

Another recent approach to anisotropic pressure evolution is the double polytropic model of *Hau et al.* [1993]. This approach uses [*Hau and Sonnerup*, 1993]

$$\frac{d}{dt}\left(\frac{p_\perp}{nB^{\gamma_\perp-1}}\right)=\frac{dC_\perp}{dt}=0, \tag{4a}$$

$$\frac{d}{dt}\left(\frac{p_\parallel B^{\gamma_\parallel-1}}{n^{\gamma_\parallel}}\right)=\frac{dC_\parallel}{dt}=0, \tag{4b}$$

where

$$C_\perp \equiv \frac{p_\perp}{nB^{\gamma_\perp-1}}, \tag{4c}$$

$$C_\parallel \equiv \frac{p_\parallel B^{\gamma_\parallel-1}}{n^{\gamma_\parallel}}, \tag{4d}$$

and where $\gamma_\perp$ and $\gamma_\parallel$ are the polytropic indices. If $\gamma_\perp$ and $\gamma_\parallel$ can be interpreted as the ratios of specific heat for perpendicular and parallel motions, respectively, it can be easily shown that equations (4a)-(4d) are essentially adiabatic equations for $p_\perp$ in terms of the 2-D motion perpendicular to magnetic flux tube and for $p_\parallel$ in terms of 1-D motion along the flux tube. If we choose $\gamma_\perp = 2$ and $\gamma_\parallel = 3$, (2a) and (2b) are obtained. On the other hand, $\gamma_\perp = 1$ ($\gamma_\parallel = 1$) leads to isothermal behavior for $T_\perp \equiv p_\perp/n$ ($T_\parallel \equiv p_\parallel/n$). From the point of view of *Hau et al.* [1993], however, $\gamma_\perp$ and $\gamma_\parallel$ are determined empirically.

The purpose of this paper is to study the structure of the magnetosheath and the associated kinetic waves/instabilities by using our 2-D global hybrid simulation. The above models of pressure anisotropy are also examined. Using data from our 2-D hybrid simulation, we will be able to study the evolution of pressure along explicit streamlines, both on and off the subsolar line. The outline of the paper is as follows. The simulation model is given in section 2. The simulation results and the analyses are given in section 3. Finally, the summary and a discussion are given in sections 4 and 5, respectively.

2. Hybrid Code Simulation Model

The 2-D ($\partial/\partial z = 0$) simulation is carried out in the geomagnetic equatorial plane, in which the x axis is assumed to be along the Sun-Earth line and pointing to the Sun and the y axis is pointing from dusk to dawn. A polar coordinate system is used in the simulation; this system consists of the radial distance r in the xy plane, the z axis pointing from north to south, and the polar angle $\theta \equiv \tan^{-1}(x/y)$. The Earth is located at the origin. The simulation domain is within the region with 10 $R_E < r <$ 25 R_E and $0° \le \theta \le 180°$. The inner boundary at $r = 10$ R_E corresponds to the magnetopause.

The 2-D hybrid code adapted in this study has been used by *Lin et al.* [1996] to simulate the interaction between the bow shock/magnetosheath and interplanetary discontinuities. In the hybrid code the ions, which are protons, are treated as discrete particles, and the electrons are treated as a massless fluid. The electrons are assumed to flow along magnetic field lines in a way that guarantees quasi charge neutrality. In our simulation the grids are uniformly distributed in the r and θ directions, with a total of 280 × 380 grid points. The grid size along the r direction is $\Delta r = 0.054$ R_E. In the calculation the ions are accelerated by electromagnetic forces. The electric field is determined from the electron momentum equation, and it is then used in Faraday's law to advance the magnetic field. The code utilizes subcycling; the magnetic field is advanced 10 times for every time the particles are advanced.

The ion gyrofrequency Ω_0 in the solar wind is chosen to be 0.5 s^{-1}, where $\Omega_0 = eB_0/m_i$, B_0 is the magnitude of the IMF, e is the electron charge, and m_i is the ion mass. This value of Ω_0 corresponds to an IMF $B_0 \simeq$ 5 nT. In the solar wind the number of ion particles per R_E^2 is chosen to be $n_0 = 6000$, and the ion inertial length $\lambda_0 \equiv c/\omega_{pi0}$, where ω_{pi0} is the ion plasma frequency, is chosen to be 0.17 R_E. The Alfvén speed in the solar wind is $V_{A0} = 0.084$ R_E s^{-1}. The electron temperature is assumed to be zero for simplicity. The ion plasma beta β_0 is chosen to be 0.5, and the ion gyroradius is ~ 0.12 R_E in the solar wind. The above value of the ion inertial length is $\sim$ 10 times the real value in the solar wind, and the Alfvén speed is $\sim$ 7 times the real value to shorten the computing time. In our simulation a total of 10,000,000 particles are used. We have also run simulations for smaller values of λ_0 and have found that the position, shape, and strength of the bow shock are nearly unchanged.

Initially, the solar wind is assumed to be uniform, and the IMF $\mathbf{B_0} = -B_0\mathbf{e_y}$ is constant in the simulation domain. The ion temperature is assumed to be isotropic. At $t = 0$ the solar wind starts to pass the obstacle, i.e., the semicircular magnetopause. The inflow speed V_0 of the solar wind is such that the magnetosonic Mach number $M_A \equiv V_0/V_{A0} = 5$. Across the front side boundary at $r = 25$ R_E the solar wind flows along the $-x$ direction and convects the IMF $\mathbf{B_0}$ into the simulation domain. The straight line boundary segments at $\theta = 0°$ and $\theta = 180°$ represent two outflow boundaries. The bow shock is formed by the interaction between the high-speed solar wind and the magnetopause. At the magnetopause boundary the tangential electric field is set to zero (perfectly conducting boundary). The time step of particle advance is $\Delta t = 0.03\Omega_0^{-1}$. Note that in the 2-D simulation the magnetic flux piles up in front of the magnetopause, which results in a longer depletion layer and a continuous slow sunward motion of the bow shock after the average jumps of physical quantities across the shock have reached a quasi steady state [*Lin et al.*, 1996]. In the present simulation some heavy diffusion of magnetic field is added within 1 R_E distance from the magnetopause boundary to reduce the pileup of the magnetic flux.

The physical quantities are normalized to the solar wind quantities as follows. The magnetic field B is normalized to B_0, the ion number density n is normalized to n_0, the flow velocity V is normalized to V_{A0}, and the time t is normalized to Ω_0^{-1}. The thermal and magnetic pressures are expressed in units of $P_0 \equiv B_0^2/\mu_0$.

3. Simulation Results and Modeling the Pressure Evolution

Figure 1 shows the magnetic field lines in the xy plane superposed on the contour plot of the magnetic field strength and the flow vectors superposed on the contour plot of the flow speed obtained from the simulation at $t = 48\Omega_0^{-1}$. For the grey-scale contour plots, the black represents the maximum value and the white represents the minimum value. The bow shock has formed at a standoff distance of $\sim 17.5\ R_E$ in front of the magnetopause. Across the front of the bow shock the azimuthal component of magnetic field increases. Correspondingly, the plasma flow speed decreases and diverges to the two flank sides. Figure 2 depicts the spatial profiles of magnetic field components B_r, B_z, and B_θ, field magnitude B, ion number density n, flow velocities V_r, V_z, and V_θ, perpendicular temperature $T_\perp$, and parallel temperature $T_\parallel$ at $t = 48\Omega_0^{-1}$ as a function of radius r. The left, middle, and right columns of Figure 2 show the profiles along the coordinate lines $\theta = 30°$, $60°$, and $90°$, respectively. The results are shown from $r = 11\ R_E$ to skip the modification by the artificial damping near the inner boundary. Note that $\theta = 90°$ is along the Sun-Earth line and that $\theta < 90°$ is in the right-hand region (dawnside) of the magnetosheath in Figure 1. It is seen that across the bow shock, which is a fast magnetosonic shock, the ion density n as well as the magnetic field strength increases nearly by a factor of 4 at $\theta = 90°$ in the subsolar region and a factor of 3 at $\theta = 30^o$. Evidence for density depletion in front of the magnetopause where the magnetic flux piles up is seen from the density profiles for $r < 14\ R_E$ at $\theta = 90°$ and $r < 16.5\ R_E$ at $\theta = 30°$. The parallel temperature is also seen to decrease in the depletion layer. At quasi-perpendicular shocks from $\theta = 60°$ to $\theta = 90°$, the enhancement in $T_\perp$ is much stronger than that in $T_\parallel$ across the shock transition. The ratio $T_\perp/T_\parallel$ then decreases in the middle region of the magnetosheath and finally goes up again in the density depletion layer. The downstream ion plasma β value ranges from ~ 0.5 to 5.

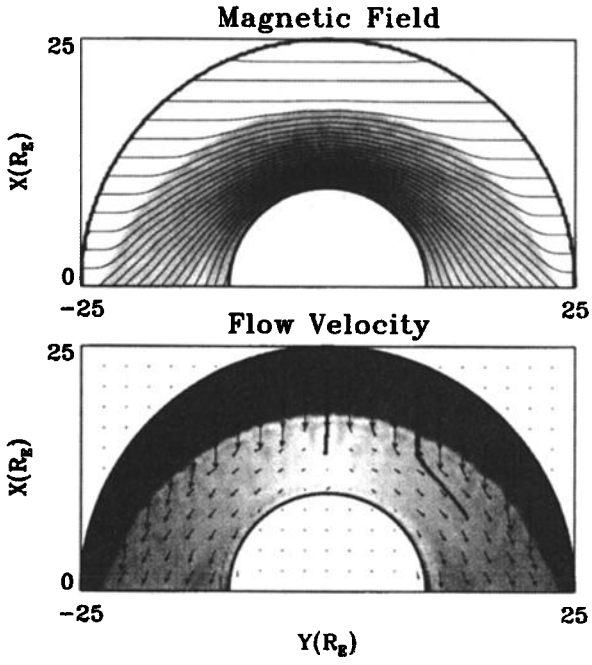

Figure 1. (top) magnetic field lines in the xy plane superposed on the contour plot of the field strength B and (bottom) flow vectors plotted on top of the contours of the flow speed obtained from the hybrid simulation at $t = 48\Omega_0^{-1}$. The IMF is oriented in the dawn-dusk ($-$y) direction, and $+x$ points to the Sun. The heavy semicircles at $r = 10\ R_E$ and $25\ R_E$ represent the simulation boundaries. The black in contour plots represents the maximum values, with $B_{\max} = 7.4B_0$ and $V_{\max} = 6.4V_{A0}$, and the white represents the minimum values, with $B_{\min} = 0.96B_0$ and $V_{\min} = 0$. The two thick curves in the bottom panel represent the streamlines analyzed in this paper, starting from $\theta = \theta_0 = 90°$ (in the center) and $60°$ (to the right), $r = r_0 = 18\ R_E$, and $t = 48\Omega_0^{-1}$.

Large, in-phase oscillations in B and n are seen immediately downstream of the quasi-perpendicular shocks near the coordinate lines with $\theta = 90°$ to $\theta = 60°$. In the deeper magnetosheath farther away from the shock front, the correlation between B and n changes from the fast-mode-like in-phase relation to an antiphase relation, as seen from Figure 2. The waves with anticorrelated B and n appear to have long wavelengths, only a few wave periods across the magnetosheath. This anticorrelation is indicative of the mirror or slow/ion acoustic mode. Transport ratio analysis [*Denton et al.*, 1995a] (not shown) suggests that these waves are the mirror mode.

We now perform analyses of the pressure evolution and wave activities for two streamlines starting from $\theta = \theta_0 = 90°$ (on the subsolar line) and $\theta = \theta_0 = 60°$ ($30°$ off the subsolar line) at radius $r = r_0 = 18\ R_E$. The streamlines, or trajectory lines, are obtained by following the convecting fluid elements with time from $t = 36\Omega_0^{-1}$ to $t = 63\Omega_0^{-1}$. The two streamlines are indicated by the thick solid curves in Figure 1. In Figure 3a we display as thick curves the proton pressure ratio $p_\perp/p_\parallel$ obtained from the hybrid simulation versus the number t^n of time steps for these two streamlines. The thin curves plotted in Figure 3a are *Anderson et al.*'s [1994] relation (3). Here and in the following, the time steps are counted starting from $t = 36\Omega_0^{-1}$. In the bow shock transition ($t^n \sim 35$ for $\theta_0 = 90°$; $t^n \sim 20$ for $\theta_0 = 60°$) the value of $p_\perp/p_\parallel$ increases to a very large value (24 for $\theta_0 = 90°$; 15 for $\theta_0 = 60°$). This large value in $p_\perp/p_\parallel$ occurs because of the specu-

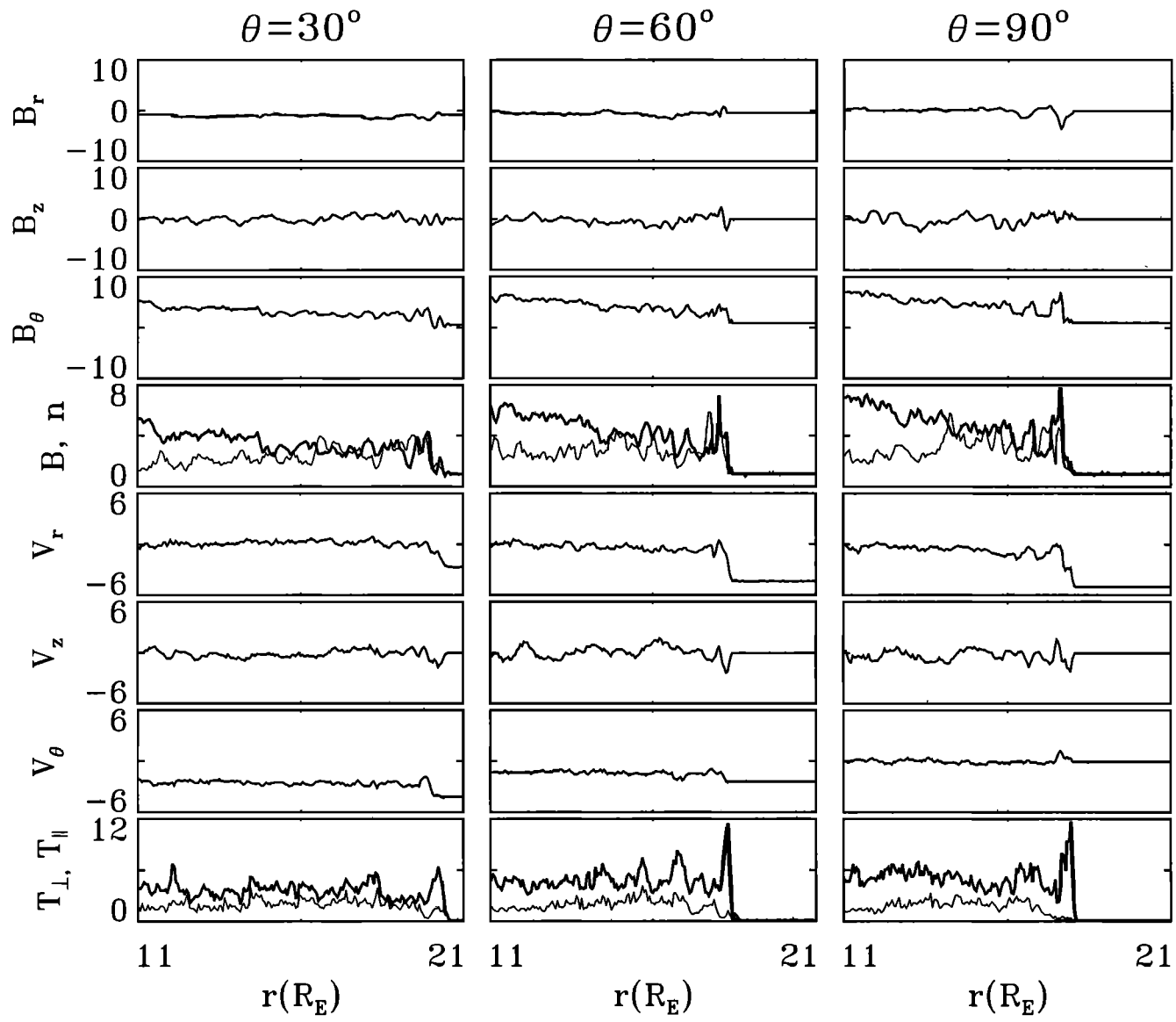

Figure 2. Spatial profiles of magnetic field components B_r, B_z, and B_θ, field magnitude B (thick curves), ion number density n (thin curves), flow velocities V_r, V_z, and V_θ, perpendicular temperature $T_\perp$ (thick curves), and parallel temperature $T_\parallel$ (thin curves) at $t = 48\Omega_0^{-1}$ as a function of radius r along the coordinate lines of (left) $\theta = 30°$, (middle) 60°, and (right) 90°. The bow shock is located at the places where n and B increase sharply and $|V_r|$ drops from its upstream solar wind value.

lar reflection at the shock; essentially, protons crossing the quasi-perpendicular bow shock with the large solar wind velocity begin to gyrate so that their bulk velocity is converted to a gyration velocity around $\boldsymbol{B}$. Some time after the bow shock crossing, $p_\perp/p_\parallel$ decreases to a moderate value ~ 2. We will attempt to model the evolution of the pressures $p_\perp$ and $p_\parallel$ after this time. The fact that $p_\perp/p_\parallel$ decreases steeply in the immediate post bow shock region is indicative of the same type of wave activity that occurs in the magnetosheath proper; however, we wish to exclude the drastic time dependence of the post bow shock plasma.

3.1. Pressure Evolution and the Double Adiabatic Theory

We now examine the double adiabatic model using our simulation data. The double adiabatic constants $C_\perp$ and $C_\parallel$ can be obtained by setting $\gamma_\perp = 2$ and $\gamma_\parallel = 3$ in (4c) and (4d). Thus for double adiabatic theory,

$$C_\perp = p_\perp/(nB), \tag{5a}$$

$$C_\parallel = p_\parallel B^2/n^3. \tag{5b}$$

The constant $C_\perp$ indicates the conservation of magnetic

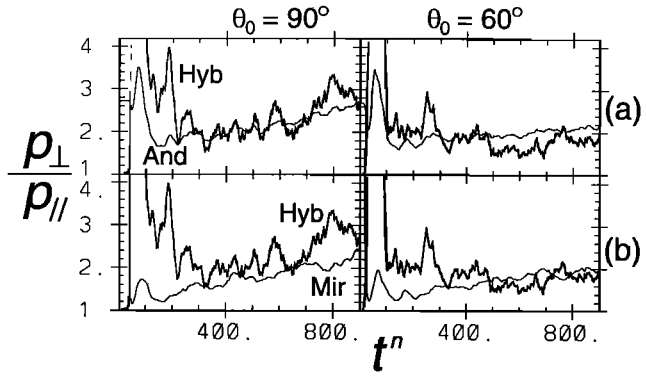

Figure 3. (a, b) The proton pressure ratio $p_\perp/p_\parallel$ from the hybrid simulation plotted versus time steps t^n (thick curves) for two streamlines, $\theta_0 = 90°$ and $\theta_0 = 60°$. The thin curve in Figure (3a) is *Anderson et al.*'s [1994] relation (3) (And), and the thin curve in Figure 3b is the mirror mode stability criterion (Mir).

moment associated with the ion perpendicular thermal speed. Combining (5a) and (5b), we can also replace the double adiabatic constant $C_\parallel$ by the conservation of the phase-space volume $C_{\rm vol}$, with

$$C_{\rm vol} = v_{\parallel th} v_{\perp th}^2/n \propto \sqrt{T_\parallel} T_\perp/n, \qquad (6)$$

where $v_{\parallel th}$ and $v_{\perp th}$ are the parallel and perpendicular thermal speeds, respectively.

Figure 4 depicts the quantities B, n, $T_\parallel$, and $T_\perp$ obtained from the simulation and the corresponding $C_{\rm vol}$ and $C_\perp$ obtained from (5a) and (6) at various time steps t^n for the two streamlines with $\theta_0 = 90°$ and $\theta_0 = 60°$. The initial time step plotted in Figure 4 is 200 (250) for $\theta_0 = 90°$ (60°). These times are large enough that the pressure ratio $p_\perp/p_\parallel$ has decreased to a moderate value ~ 2, as seen in Figure 3. The quantities $C_{\rm vol}$ and $C_\perp$ are found oscillating along the streamlines. For the 90° streamline, $C_{\rm vol}$ increases from $t^n = 270$ and then decreases from the peak value at $t^n = 320$, followed by some smaller amplitude oscillations. These oscillations may be due to energy exchange with waves. The variation in $C_\perp$ is not as large as that in $C_{\rm vol}$. The decrease in the phase-space volume $C_{\rm vol}$ is found to occur with the decrease in $T_\parallel$ and thus the parallel thermal speed $v_{\parallel th}$. The percent change in $T_\perp$ is not as large as that in $T_\parallel$, because $T_\perp/T_\parallel > 1$. At the times that $T_\parallel$ reaches a minimum, the perpendicular to parallel temperature ratio is found to reach a maximum value that even exceeds the upper bound from *Anderson et al.*'s [1994] formula (3), as can be seen from the thin curve in the left column of Figure 3a. Throughout the time period the magnetic field B shows a nearly monotonic increase.

For the streamline with $\theta_0 = 60°$ the phase space volume $C_{\rm vol}$ peaks significantly around $t^n = 500$ and decreases significantly at $t^n > 700$. Correspondingly, both $T_\parallel$ and $T_\perp$ reach a minimum at $t^n > 700$. The increase in $C_{\rm vol}$ at $t^n \simeq 500$ is mainly caused by the peak in $T_\parallel$ and the decrease in n. The increase in $T_\parallel$ at this time is found to occur right after the peak in $T_\perp/T_\parallel$ (near $t^n = 420$) that exceeds the upper bound ratio from *Anderson et al.*'s [1994] formula. The decrease in n at $t^n > 400$ marks the entrance into the density depletion region, as seen from the density structure along the 60° streamline. Around the flanks, the plasma downstream of the quasi-parallel shock has lower pressure. The connection to the plasma at the boundary may lead to a negative contribution to $p_\parallel$ from the third moment and thus a decrease in $T_\parallel$ at $t^n > 700$.

The fact that $C_{\rm vol}$ and $C_\perp$ are not constant indicates that there may be particle pitch angle scattering due to wave activity in the magnetosheath or parallel heat conduction that violates the adiabatic conditions. The energy exchange from $p_\perp$ to $p_\parallel$ due to ion-cyclotron instabilities will be discussed later in sections 3.2 and 3.3. However, we note now that in a plasma with $T_\perp > T_\parallel$, energy exchange from $T_\perp$ to $T_\parallel$ (which occurs when the waves take energy from the particle distribution) only leads to an increase in $C_{\rm vol}$, and the change in $C_{\rm vol}$ is proportional to $(T_\perp - T_\parallel)$. (This is found by differentiating $C_{\rm vol}$ with respect to $d\Delta p$, where Δp is defined in (14).) Thus oscillations in $C_{\rm vol}$ may imply some back and forth transfer of energy between waves and particles.

Because of the compression of magnetic flux tubes in front of the magnetopause, which is stronger in the

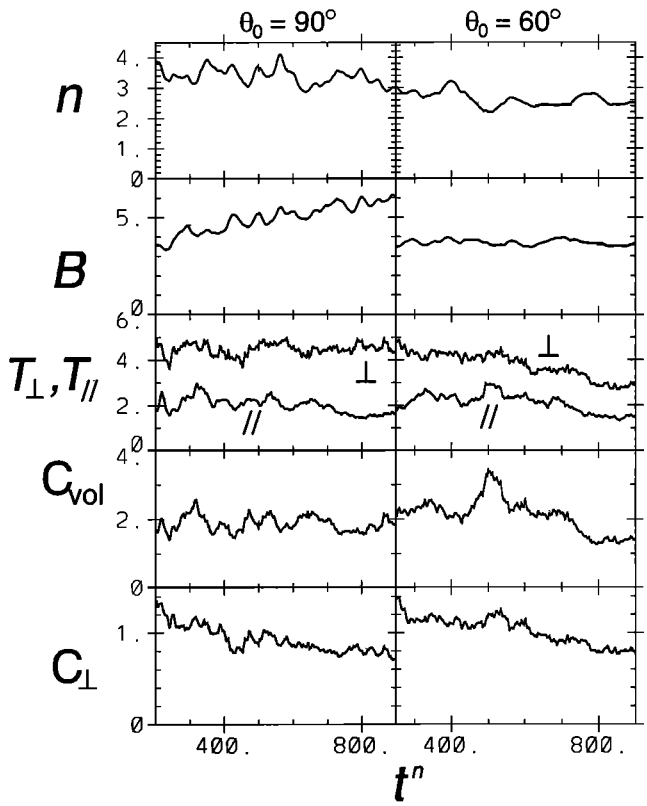

Figure 4. Quantities n, B, $T_\parallel$, and $T_\perp$ obtained from the simulation and the corresponding $C_{\rm vol}$ and $C_\perp$ obtained from (5a) and (6) at various time steps t^n for the two streamlines with $\theta_0 = 90°$ and 60°.

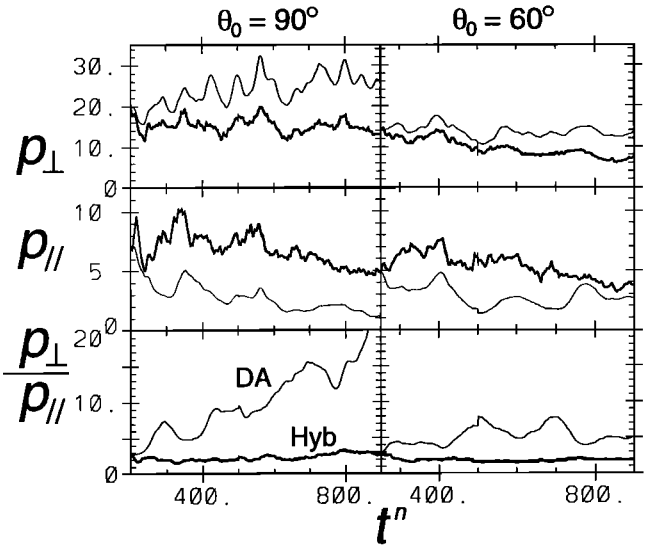

Figure 5. The perpendicular and parallel proton pressure, $p_\perp$ and $p_\parallel$, respectively, and proton pressure ratio $p_\perp/p_\parallel$ obtained in the hybrid simulation (Hyb) versus time t^n (thick curves) in simulation units for the two streamlines $\theta_0 = 90°$ and 60°. The thin curves show the prediction of the double adiabatic theory (DA) for $p_\perp$ and $p_\parallel$ using their initial values from the hybrid simulation and the double adiabatic equations (2).

subsolar magnetosheath where the flow vector is normal to the magnetopause and thus the normal pressure is relatively high, particles with high parallel speeds toward the two flanks may be squeezed out of the magnetosheath within the transient convection time. Suppose that the significant decrease in $C_{\rm vol}$ at $t^n > 700$ is due to the parallel heat loss. We can estimate this decrease in $C_{\rm vol}$ by considering the loss of the particles which have a high-speed parallel to the magnetic field from an initial population with a thermal speed $v_{\parallel th}$. Consider the net effects of the heat conduction at a local volume to be loss of heat. Assume that $T_\perp$ is nearly constant and that a number dn particles with a parallel speed $v_\parallel = v_l > v_{\parallel th}$ are lost from a local magnetosheath region. The parallel thermal speed of the new phase-space population can be estimated as

$$v'^2_{\parallel th} = [nv^2_{\parallel th} - (dn)v_l^2]/(n - dn). \quad (7)$$

The ratio of the new $C'^2_{\rm vol}$ to the initial $C^2_{\rm vol}$ can be written as

$$C'^2_{\rm vol}/C^2_{\rm vol} = [n^2/(n-dn)^2][nv^2_{\parallel th} - (dn)v_l^2]/[(n-dn)v^2_{\parallel th}]. \quad (8)$$

The phase-space volume $C'_{\rm vol} < C_{\rm vol}$ if $v_l^2 > 3(1 - dn/n)v^2_{\parallel th}$. For $dn/n \sim 25\%$ and $C'^2_{\rm vol}/C^2_{\rm vol} \sim 0.3$, as on the 60° streamline for the overall change through the density depletion region, the speed v_l is estimated to be $1.9v_{\parallel th}$. Taking into account the decrease in $T_\perp$, the required speed v_l is nearly $1.6v_{\parallel th}$.

A major purpose of this paper is to examine the currently existing models of pressure evolution in the magnetosheath with our simulation data. Now we investigate the pressure evolution along the streamlines and compare it to the double adiabatic theory. Figure 5 displays as thick curves the quantities $p_\perp$, $p_\parallel$, and the proton pressure ratio $p_\perp/p_\parallel$ in the hybrid simulation versus time step t^n for the two streamlines with $\theta_0 = 90°$ and 60°. The thin curves in Figure 5 represent the results of double adiabatic theory obtained in the following way. First, the constants $C_\perp$ and $C_\parallel$ at the initial time are calculated according to (2) using the values $p_\perp$, $p_\parallel$, n, and B from the hybrid simulation. Then, at later times, we keep the values of $C_\perp$ and $C_\parallel$ constant and find the double adiabatic values $p_{\perp DA}$ and $p_{\parallel DA}$ from $p_{\perp DA} = C_\perp nB$ and $p_{\parallel DA} = C_\parallel n^3/B^2$, respectively, using the time-dependent values of n and B from the hybrid simulation.

In the case of the $\theta_0 = 90°$ (subsolar line) data, n decreases while B increases (Figure 4). This leads to a steep decrease in the double adiabatic value $p_{\parallel DA}$, as seen from (5b). Since B increases proportionately more than n, $p_{\perp DA}$ rises somewhat (see equation (5a)). Thus $(p_\perp/p_\parallel)_{DA}$ increases very steeply, as shown in Figure 5. Clearly, the double adiabatic theory is not adequate to describe the evolution of the anisotropic pressures in the $\theta_0 = 90°$ case. In the $\theta_0 = 60°$ case, n decreases only slightly while B is almost constant over the time period displayed in Figure 5. While $p_{\perp DA}$ remains nearly constant, $p_\perp$ in the hybrid simulation decreases. Because of the steeper dependence of $p_{\parallel DA}$ on n, as seen from (5b), $p_{\parallel DA}$ decreases. The value of $p_\parallel$ in the simulation also decreases a similar amount overall, although at intermediate times the curves for $p_\parallel$ of the hybrid simulation and $p_{\parallel DA}$ from the double adiabatic fit in Figure 5 are quite different.

3.2. Evidence for Wave Activity

From Figure 3a we see that the hybrid simulation $p_\perp/p_\parallel$, after rising to a very large value, falls to a value near that of (3) along both streamlines and stays near or below that value. Since (3) represents a condition close to marginal stability for the proton cyclotron wave [*Denton et al.*, 1994; *Gary et al.*, 1994], the fact that $p_\perp/p_\parallel$ falls to a value near (3) is indicative of the effect of proton cyclotron waves. The thin curve plotted in Figure 3b is the mirror mode stability criterion

$$\left(\frac{p_\perp}{p_\parallel}\right)_{\rm Mir} = 1 + \frac{1}{\beta_\perp}. \quad (9)$$

Comparing Figures 3a and 3b, it is clear that $(p_\perp/p_\parallel)_{\rm Mir}$ lies under but close to $(p_\perp/p_\parallel)_{\rm And}$. Some evidence suggests that the proton cyclotron mode rather than the mirror mode plays the major role in regulating the pressure ratio $p_\perp/p_\parallel$ in the magnetosheath (see references in the work of *Denton et al.* [1994]), but the mirror

mode could also be playing some role [see also *Hill et al.*, 1995].

Besides the fact that $p_\perp/p_\parallel$ in the hybrid simulation lies close to $(p_\perp/p_\parallel)_{\rm And}$, further evidence for wave pitch angle scattering comes from the fact that the hybrid code $p_\perp$ increases less than the double adiabatic value $p_{\perp DA}$, and the hybrid code $p_\parallel$ decreases less than $p_{\parallel DA}$, as shown in Figure 5. This may indicate pitch angle scattering which transfers energy continually from $p_\perp$ to $p_\parallel$ in the hybrid simulation. Note that this is the basic idea of the bounded anisotropy model [*Denton et al.*, 1994, 1995b], which combines double adiabatic driving terms with energy transfer from $p_\perp$ to $p_\parallel$.

We have also conducted an analysis of wave modes present in our hybrid simulation of the magnetosheath. In a low-frequency plasma in which $\omega \ll \Omega_p$, where Ω_p is the ion gyrofrequency, kinetic theory yields four basic modes, the three waves corresponding to the normal modes of MHD theory and the mirror mode. The mirror mode has zero phase velocity in a homogeneous plasma (though it can acquire a finite phase velocity when there is inhomogeneity [*Johnson and Cheng*, 1997]). The three modes with finite phase velocity are the magnetosonic/fast/whistler mode, the Alfvén/ion-cyclotron mode, and the ion-acoustic/slow/sound mode [*Krauss-Varban et al.*, 1994; *Denton et al.*, 1995a].

The waves in the simulation can be identified using polarization information and the following transport ratios [*Denton et al.*, 1995a, 1998, and references therein]. The compressibility of ions is given by

$$C(\mathbf{k},\omega) \equiv \frac{\langle \delta n \delta n \rangle_{\mathbf{k}\omega}}{\bar{n}^2} \frac{\bar{B}^2}{\langle \delta \mathbf{B} \cdot \delta \mathbf{B} \rangle_{\mathbf{k}\omega}}, \qquad (10)$$

where $\mathbf{k}$ is the wave vector, ω is the angular frequency, $\bar{B}$ and $\bar{n}$ are the low-frequency ("equilibrium") components of the magnetic field and ion density, respectively, and $\delta \boldsymbol{B}$ and δn are the fluctuating components. The Alfvén ratio is given by

$$R_A(\mathbf{k},\omega) \equiv \frac{\langle \delta \mathbf{v} \cdot \delta \mathbf{v} \rangle_{\mathbf{k}\omega}}{\bar{V}_A^2} \frac{\bar{B}^2}{\langle \delta \mathbf{B} \cdot \delta \mathbf{B} \rangle_{\mathbf{k}\omega}}, \qquad (11)$$

where $\bar{V}_A \equiv \bar{B}/\sqrt{4\pi \bar{n} m_i}$ is the Alfvén speed. The parallel phase ratio is given by

$$R_{\parallel n}(\mathbf{k},\omega) \equiv \frac{\langle \delta n \delta B_\parallel \rangle_{\mathbf{k}\omega}}{\sqrt{\langle \delta n \delta n \rangle_{\mathbf{k}\omega} \langle \delta B_\parallel \delta B_\parallel \rangle_{\mathbf{k}\omega}}}, \qquad (12)$$

which is equivalent to the cosine of the phase angle between the fluctuating component $\delta B_\parallel$ and δn. The magnetic compressibility can be written as

$$C_B(\mathbf{k},\omega) \equiv \frac{\langle \delta B_\parallel \delta B_\parallel \rangle_{\mathbf{k}\omega}}{\langle \delta \mathbf{B} \cdot \delta \mathbf{B} \rangle_{\mathbf{k}\omega}}. \qquad (13)$$

For the two convection streamlines with $\theta_0 = 90°$ and $\theta_0 = 60°$ (starting from $t^n = 200$ and 250, respectively), we Fourier transform the data in time and plot

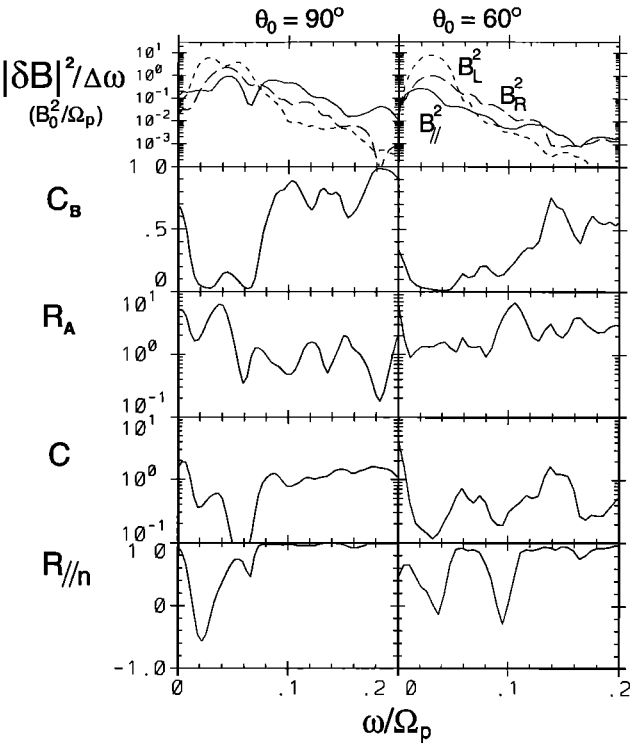

Figure 6. Power spectra of the magnetic field fluctuations $|\delta B|^2/\Delta\omega$, the magnetic compressibility C_B, the Alfvén ratio R_A, the compressibility C, and the parallel phase ratio $R_{\parallel n}$ as a function of angular frequency, ω/Ω_p, for the streamlines $\theta_0 = 90°$ and 60°. The power spectra are given for parallel fluctuations (solid curve), right-hand-polarized fluctuations (long dashed curve), and left-hand-polarized fluctuations (short dashed curve).

in Figure 6 the power spectrum of the magnetic field $|\delta B|^2/\Delta\omega$ as well as C_B, R_A, C, and $R_{\parallel n}$ as a function of angular frequency normalized to the local cyclotron frequency, ω/Ω_p. The power spectra are given for parallel fluctuations, right-hand-polarized fluctuations, and left-hand-polarized fluctuations. The power spectra show that at very low frequencies ($\omega/\Omega_p < 0.06$), there are dominant fluctuations with left-hand polarization. In this frequency range, C_B is low, consistent with the dominant left-hand power. The Alfvén ratio R_A is close to unity, indicating equal velocity and magnetic fluctuations when normalized to $\bar{V}_A$ and $\bar{B}$, respectively. The compressibility C is small compared to unity, indicating a low level of density fluctuations. These features are characteristic of Alfvén waves. Using the mode identification method of *Denton et al.* [1995a, 1998] we find that these waves are well identified as either the quasi-parallel Alfvén/ion-cyclotron or the quasi-parallel magnetosonic/fast/whistler mode (the quasi-parallel mode is also Alfvén-like). With the additional information that the waves are left-hand-polarized, we can confidently identify these waves as the quasi-parallel Alfvén/ion-cyclotron mode. These waves are most likely produced by the ion-cyclotron instability

which is driven by the anisotropy of the plasma pressure.

At higher frequencies there are dominant parallel fluctuations for the $\theta_0 = 90°$ streamline (at $\omega/\Omega_p > 0.08$) and a mixture of parallel and right-hand-polarized fluctuations for $\theta_0 = 60°$ (at $\omega/\Omega_p > 0.12$). Looking at the $\theta_0 = 90°$ characteristics, we see from Figure 6 that C_B is large, R_A is of order unity, C is about unity, and $R_{\|n} = +1$. The latter two quantities indicate that the relative density and magnetic fluctuations are of the same magnitude and in phase, which is characteristic of the quasi-perpendicular magnetosonic/fast mode. In fact, these waves are well identified as the quasi-perpendicular magnetosonic/fast mode using the method of *Denton et al.* [1995a], as are the higher-frequency waves for the $\theta_0 = 60°$ case. The fast mode has purely parallel magnetic fluctuations only for $\boldsymbol{k}$ perpendicular to $\boldsymbol{B}$. For parallel propagation the mode is right-hand-polarized. The fact that there is a significant amount of right-hand-polarized power for $\theta_0 = 60°$ probably indicates that the waves are oblique ($\boldsymbol{k}$ is oblique to $\boldsymbol{B}$). Such a result is easily understood if we regard these waves as fast mode waves reflecting off the inner magnetopause boundary. Along the $\theta_0 = 90°$ streamline, which is nearly the Sun-Earth line, the reflected waves would propagate directly back along the same line, and $\boldsymbol{k}$ would be perpendicular to $\boldsymbol{B}$. Off the Sun-Earth line, the waves would reflect at some angle to the Sun-Earth line, and this angle will, in general, be oblique to the local $\boldsymbol{B}$.

There is no indication of the mirror mode in Figure 6. This is not completely surprising considering that the ordinary (infinite homogeneous) mirror mode has zero frequency and would not show up as an oscillation in the rest frame of the plasma (along streamlines). We have done transport ratio analysis using spatially varying data at fixed time (such as that in Figure 2). Note in Figure 2 the out-of-phase fluctuations in density and magnetic field amplitude to the left of the figure (toward the magnetopause). Conclusive identification of the mirror mode by this means is difficult because of the large variation in wavelength of the mode across the simulation. Another complicating factor is the simultaneous presence of perpendicularly polarized (Alfvén-like) magnetic fluctuations. Nevertheless, the transport ratio analysis (not shown) is suggestive that the out-of-phase density and magnetic fluctuations seen in Figure 2 result from the mirror mode. These waves are observed in the spatial variation and are presumably at very low frequency in the temporal domain; they should not be confused with the compressional waves discussed above with $\omega/\Omega_p > 0.1$ which were identified as the quasi-perpendicular magnetosonic/fast mode.

Observations indicate that there is spatial variation of modes across the magnetosheath [*Hubert*, 1994; *Anderson et al.*, 1994; *Song et al.*, 1994; *Hubert et al.*, 1998; *Denton*, 2000]. Breaking up the time series used for the transport ratio analysis into three segments (starting right after the bow shock crossing) and redoing the analysis for each segment, we find the following results: Near the bow shock, it appears that the power in the Alfvén/ion-cyclotron and quasi-perpendicular/fast modes is comparable, with the power of both peaked at $\omega/\Omega_p < 0.1$. Farther away from the bow shock, the Alfvén/ion-cyclotron power increases and dominates the total power (Figure 6; the power of this mode is greatest in the middle segment). At the same time, the quasi-perpendicular/fast mode power decreases overall but increases for $\omega/\Omega_p > 0.1$. As has been noted from the spatially varying data of Figure 2, it appears that there are quasi-perpendicular/fast waves near the bow shock (consistent with the result just mentioned) and the mirror mode farther away from the bow shock (which would not be expected to be observed in the streamline data).

3.3. Examination of Bounded Anisotropy Model

To test the bounded anisotropy model, we started with the same initial plasma conditions which we used to examine the double adiabatic theory at $t^n = 200$ (250) for the $\theta_0 = 90°$ (60°) case. The bounded anisotropy values of $p_\perp$ and $p_\|$, $p_{\perp\mathrm{BAM}}$ and $p_{\|\mathrm{BAM}}$, respectively, were given the initial values of $p_\perp$ and $p_\|$ from the hybrid simulation and then allowed to evolve according to the bounded anisotropy model. The bounded anisotropy model, in its simplest formulation, is a two-step process [*Denton and Lyon*, 1996]. In each time step, the double adiabatic equations (2a) and (2b) are first used to advance ${p_\|}^n$ and ${p_\perp}^n$ (time step n) to tentative values ${p_\|}^*$ and ${p_\perp}^*$; then, if the pressure ratio ${p_\perp}^*/{p_\|}^*$ exceeds the bound implied by (3) (a function of the tentative ${p_\|}^*$ through $\beta_\|$), a local exchange of energy at each grid point is made to find the new pressure values for time step $n+1$,

$$ {p_\|}^{n+1} = {p_\|}^* + 2\Delta p, \tag{14a} $$

$$ {p_\perp}^{n+1} = {p_\perp}^* - \Delta p, \tag{14b} $$

such that the new pressure ratio ${p_\perp}^{n+1}/{p_\|}^{n+1}$ lies on the bound implied by (3) (with $\beta_\|$ now a function of ${p_\|}^{n+1}$).

Figure 7 shows as thin curves the time-evolved values of $p_{\perp\mathrm{BAM}}$, $p_{\|\mathrm{BAM}}$, and $(p_\perp/p_\|)_{\mathrm{BAM}}$ (lower thin curve). Also shown as thin curves are the double adiabatic parameters (equation (5)) $C_{\perp\mathrm{BAM}}$ and $C_{\|\mathrm{BAM}}$ given as a function of $p_{\perp\mathrm{BAM}}$ and $p_{\|\mathrm{BAM}}$. Owing to the energy exchange, these are not constant. The thick curves in Figure 7 represent values from the hybrid simulation. In the panel for $p_\perp/p_\|$ the upper thin curve is $(p_\perp/p_\|)_{\mathrm{And}}$ evaluated from *Anderson et al.*'s [1994] formula (3) using $p_{\|\mathrm{BAM}}$ for $\beta_\|$. The bounded anisotropy model seems to do a fairly good job of predicting the evolution of $p_\perp$ (except perhaps for $\theta_0 = 60°$ at large times). The bounded anisotropy model seems to predict the overall downward trend for $p_\|$, but the oscil-

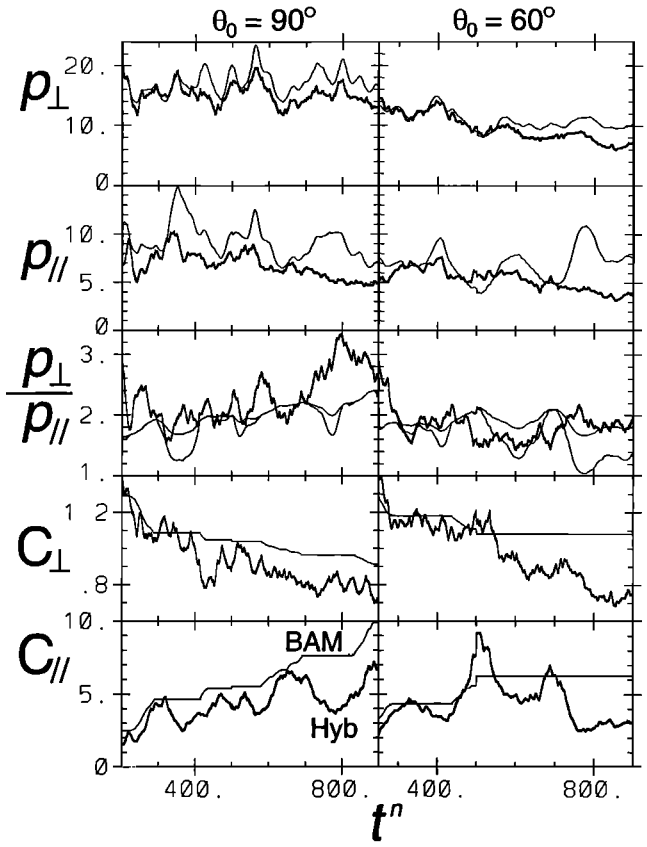

Figure 7. Perpendicular and parallel pressures $p_\perp$ and $p_\parallel$, pressure ratio $p_\perp/p_\parallel$, and double adiabatic parameters $C_\perp$ and $C_\parallel$ (equation (5)) versus time t^n for the bounded anisotropy model (BAM, indicated by thin curves) and hybrid simulation (Hyb, indicated by thick curves) and for the two streamlines $\theta_0 = 90°$ and 60°. The upper thin curve for $p_\perp/p_\parallel$ is the Anderson formula (3) evaluated using $p_{\parallel\mathrm{BAM}}$ in $\beta_\parallel$.

lations to large values of $p_{\parallel\mathrm{BAM}}$ and the final value of $p_{\parallel\mathrm{BAM}}$ for $\theta_0 = 60°$ are not consistent with $p_\parallel$ from the hybrid simulation. The plot of $p_\perp/p_\parallel$ in Figure 7 is very helpful for understanding the energy exchange process in the bounded anisotropy model. It is only when the lower thin curve representing $(p_\perp/p_\parallel)_{\mathrm{BAM}}$ becomes coincident with the upper thin curve representing $(p_\perp/p_\parallel)_{\mathrm{And}}$ (equation (3)) that energy exchange can take place. The first time period of energy exchange for $\theta_0 = 90°$ is from $t^n = 230$ to ~ 300. Noting that $C_\perp \propto p_\perp$ and $C_\parallel \propto p_\parallel$ (equation (5)), the decrease in $C_{\perp\mathrm{BAM}}$ along with an increase in $C_{\parallel\mathrm{BAM}}$ also indicates an exchange of energy from $p_{\perp\mathrm{BAM}}$ to $p_{\parallel\mathrm{BAM}}$ as in (14). The overall trend of decreasing $C_\perp$ and increasing $C_\parallel$ is predicted by the bounded anisotropy model, though there are some significant differences between the model and hybrid code values.

One of the greatest differences in the bounded anisotropy and hybrid code results displayed in Figure 7 is the fact that the large increases in $p_{\parallel\mathrm{BAM}}$ predicted by the bounded anisotropy model are not observed in $p_\parallel$ from the hybrid simulation. Considering the $\theta_0 = 90°$ case, large increases in $p_{\parallel\mathrm{BAM}}$ occur at $t^n = 350$, 570, and 780. The increases in $p_{\parallel\mathrm{BAM}}$ occur during periods of no energy exchange as evidenced by the constant values of $C_{\perp\mathrm{BAM}}$ and $C_{\parallel\mathrm{BAM}}$ at these times. (Since it is the decreasing $p_\parallel$ which leads to increased $p_\perp/p_\parallel$ and therefore to waves, it is better to think of the energy exchange as a braking effect which keeps $p_\parallel$ from decreasing rather than as a source of energy to make $p_\parallel$ increase.) Thus the increase in $p_{\parallel\mathrm{BAM}}$ is required to keep $C_{\parallel\mathrm{BAM}}$ constant (see equation (5b)). When large increases are predicted for $p_{\parallel\mathrm{BAM}}$ but not observed in $p_{\parallel\mathrm{Hyb}}$, there is a dip in $C_\parallel$ from the hybrid simulation. It is impossible for the bounded anisotropy model to predict such a decrease, or to predict an increase in $C_\perp$ for that matter. The only thing in the bounded anisotropy model which can change the values of $C_\perp$ and $C_\parallel$ is energy exchange, and the only energy exchange allowed is from $p_\perp$ to $p_\parallel$, leading to a decrease of $C_\perp$ and an increase of $C_\parallel$. The fact that there are peaks in $p_{\parallel\mathrm{Hyb}}$ indicates that the double adiabatic driving terms are playing a role (note also the peaks in $p_{\parallel DA}$ in Figure 5). The peaks in $p_{\parallel\mathrm{Hyb}}$ may be lower because of damping of the oscillations due to the parallel heat flux, or there might be a reverse flow of energy from $p_{\parallel\mathrm{Hyb}}$ to $p_{\perp\mathrm{Hyb}}$ due to damped ion-cyclotron waves.

The best agreement between $p_{\parallel\mathrm{BAM}}$ and $p_{\parallel\mathrm{Hyb}}$ occurs during the periods of energy exchange; it is at these times that $p_{\parallel\mathrm{BAM}}$ is at its lowest values. During energy exchange, the value of $p_{\parallel\mathrm{BAM}}$ is coupled to that of $p_{\perp\mathrm{BAM}}$ for which there is a better agreement with $p_\perp$ from the hybrid simulation. Furthermore, there is greater energy in $p_\perp$ than in $p_\parallel$ ($p_\perp/p_\parallel > 1$), so the coupling of $p_\parallel$ to $p_\perp$ contributes to the better agreement in $p_{\parallel\mathrm{BAM}}$ and $p_{\parallel\mathrm{Hyb}}$ during those times.

Another difference in the bounded anisotropy and hybrid results is that the value of $(p_\perp/p_\parallel)_{\mathrm{BAM}}$ averaged over the oscillation timescale ($\sim$ 100–200 steps) is greater than that of $p_\perp/p_\parallel$ in the hybrid simulation. The agreement with the BAM model in Figure 7 can be improved slightly by taking $(p_\perp/p_\parallel)_{\mathrm{And}} \leq 1 + \beta_\parallel^{-.5}$ (not shown) rather than $(p_\perp/p_\parallel)_{\mathrm{And}} \leq 1 + 0.85\beta_\parallel^{-.5}$.

Consider now the $\theta_0 = 60°$ case. The results for $t^n \leq 700$ are similar to those for $\theta_0 = 90°$. After $t^n = 700$ there is a large increase in the predicted $p_{\parallel\mathrm{BAM}}$. Though $p_{\parallel\mathrm{BAM}}$ decreases at $t^n \sim 850$, it shows no sign of decreasing to the value of $p_\parallel$ from the hybrid simulation. It is interesting to note that $C_{\perp\mathrm{BAM}}$ and $C_{\parallel\mathrm{BAM}}$ are constant after $t^n = 500$. The simultaneous drop in $C_\perp$ and $C_\parallel$ of the hybrid simulation from $t^n \sim 500$ to $t^n = 900$ cannot be explained by the bounded anisotropy model.

In order to see how well the bounded anisotropy model can describe the evolution of $p_\perp$ apart from the effect of the modeled $p_\parallel$, we have also used the bounded anisotropy model to get $p_\perp$ with $p_{\parallel\mathrm{BAM}}$ set equal to $p_\parallel$ of the hybrid simulation. The net effect is that $p_{\perp\mathrm{BAM}_\perp}$ evolves according to double adiabatic theory if $p_{\perp\mathrm{BAM}_\perp}/p_\parallel < (p_\perp/p_\parallel)_{\mathrm{And}}$, but $p_{\perp\mathrm{BAM}_\perp}$ is not allowed

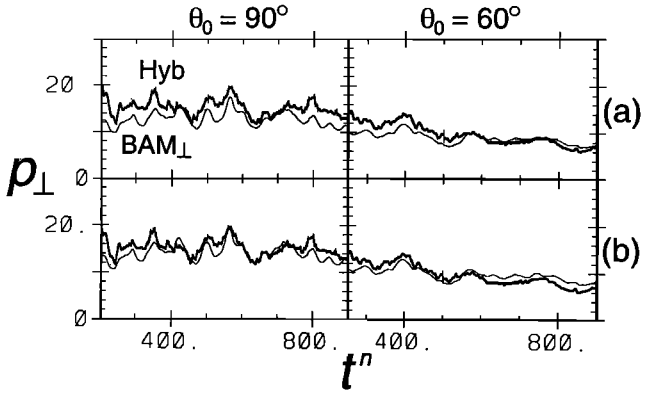

Figure 8. Bounded anisotropy solution for the perpendicular pressure $p_{\perp \mathrm{BAM}_\perp}$ only (thin curve) with $p_\perp$ from the hybrid simulation (thick curve) versus t^n for $\theta_0 = 90°$ and $\theta_0 = 60°$. The value of $p_{\perp \mathrm{BAM}_\perp}$ is limited to (a) $\leq p_\parallel(1 + 0.85\beta_\parallel^{-.5})$ or (b) $\leq p_\parallel(1 + \beta_\parallel^{-.5})$. The solution here differs from that of Figure 7 in that the model $p_\parallel$ is simply equated to the hybrid simulation value $p_\parallel$.

to become so large that $p_{\perp \mathrm{BAM}_\perp}/p_\parallel > (p_\perp/p_\parallel)_{\mathrm{And}}$. In Figure 8a we plot $p_{\perp \mathrm{BAM}_\perp}$ along with $p_\perp$ from the hybrid code versus time for $\theta_0 = 90°$ and $\theta_0 = 60°$. In Figure 8a we have used $(p_\perp/p_\parallel)_{\mathrm{And}} \leq 1 + 0.85\beta_\parallel^{-.5}$ as in (3). The resulting $p_{\perp \mathrm{BAM}}$ agrees very well with $p_\perp$ of the hybrid simulation. Even better agreement between the two is found using $(p_\perp/p_\parallel)_{\mathrm{And}} \leq 1 + \beta_\parallel^{-.5}$. Results for this case are shown in Figure 8b.

The good agreement between the $p_{\perp \mathrm{BAM}_\perp}$ from the bounded anisotropy model and the $p_\perp$ from the hybrid simulation leads us to believe that the bounded anisotropy model describes $p_\perp$ very well, and that energy exchange due to wave pitch angle scattering is occurring. However, something seems to be missing in the description of $p_\parallel$. It is most likely that the parallel heat flux, proportional to the third moment of the particle velocity relative to the mean flow, leads to a significant contribution to the evolution of $p_\parallel$ in the hybrid simulation, as discussed in section 3.1. The heat flux could be drawing energy out of the system, thereby leading to the simultaneous drop of $C_\perp$ and $C_\parallel$ observed for $\theta_0 = 60°$; the heat flux could also be damping the oscillations of $p_{\parallel \mathrm{BAM}}$, leading to much reduced oscillations in $p_{\parallel \mathrm{Hyb}}$. Another effect missing in the bounded anisotropy model is time-dependent regulation of the pressure anisotropy by waves, which will be discussed further in section 4. Waves may even give back energy to the particles, possibly leading to the oscillations in C_{vol} discussed in section 3.1.

3.4. Sensitivity to Initial Conditions

There is some sensitivity of our results to the initial time chosen for the evolution of the model pressure values. We have chosen $t^n = 200$ and 250 as the starting times for $\theta_0 = 90°$ and 60°, respectively. Generally, as expected, the agreement between the models and the hybrid code results will be better if we start the model evolution later (and so evolve the pressures for less time), regardless of the model. If we start the evolution of pressures at $t^n = 300$, the double adiabatic model appears to do just as good a job at describing the evolution of $p_\parallel$ as the bounded anisotropy model does. The value of $p_\perp$, however, is better described by the bounded anisotropy model (deviations from the hybrid results of $\sim 20\%$ versus $\sim 40\%$ for $p_{\perp DA}$). The greatest difference in results is for the pressure ratio; $(p_\perp/p_\parallel)_{DA}$ is off from $(p_\perp/p_\parallel)_{\mathrm{Hyb}}$ by a factor of 2 by the end of the simulation ($t^n = 900$), while $(p_\perp/p_\parallel)_{\mathrm{BAM}}$ is only off by $\sim 20\%$.

The bounded anisotropy model gives results which are far better than double adiabatic theory if we start the pressure evolution at even earlier times than those chosen for this paper. If we start the $\theta_0 = 90°$ simulation at $t^n = 60$, by the end of the simulation ($t^n = 900$), $(p_\perp/p_\parallel)_{DA}$ is greater than $(p_\perp/p_\parallel)_{\mathrm{Hyb}}$ by a factor of 30 ($(p_\perp/p_\parallel)_{DA} > 100$, owing to a large drop in $p_{\parallel DA}$), while $(p_\perp/p_\parallel)_{\mathrm{BAM}}$ varies from $(p_\perp/p_\parallel)_{\mathrm{Hyb}}$ by only 27%. In fact, it is clear that it is the time period just after the bow shock crossing, where $(p_\perp/p_\parallel)_{\mathrm{Hyb}}$ is very large, for which the kind of energy exchange modeled by the bounded anisotropy model will play the greatest role. On the other hand, the bounded anisotropy model in its current form will not do a very good job of modeling the highly time dependent transition from $(p_\perp/p_\parallel)_{\mathrm{Hyb}} \gg 1$ to $(p_\perp/p_\parallel)_{\mathrm{Hyb}} \sim (p_\perp/p_\parallel)_{\mathrm{And}}$, since it assumes that the waves are always regulating $p_\perp/p_\parallel$ to be at or under $(p_\perp/p_\parallel)_{\mathrm{And}}$. If the model pressure evolution is started at $t^n = 60$, by $t^n = 900$, $p_{\perp \mathrm{BAM}}$ is larger than $p_{\perp \mathrm{Hyb}}$ by $\sim 50\%$, and $p_{\parallel \mathrm{BAM}}$ is larger than $p_{\parallel \mathrm{Hyb}}$ by $\sim 18\%$ (which is still a far better agreement than the double adiabatic theory yields).

3.5. Double Polytropic Model

We have also tested the double polytropic model [*Hau et al.*, 1993] using the hybrid simulation results. The values of $\gamma_\perp$ and $\gamma_\parallel$ were chosen to minimize the standard deviation in the respective $C_\perp/\langle C_\perp\rangle$ and $C_\parallel/\langle C_\parallel\rangle$. Here $\langle C_\perp\rangle$ and $\langle C_\parallel\rangle$ are the values of $C_\perp$ and $C_\parallel$ averaged over t, and $C_\parallel/\langle C_\parallel\rangle$ are calculated using n, B, $p_\perp$, and $p_\parallel$ from the hybrid simulation. The values of $\gamma_\perp$ and $\gamma_\parallel$ and the standard deviations in the respective $C_\perp/\langle C_\perp\rangle$ and $C_\parallel/\langle C_\parallel\rangle$ are listed in Table 1. From Table 1 we see that for $\theta_0 = 90°$, the optimal $\gamma_\perp \simeq 1$, indicating that the perpendicular pressure is approximately isothermal with $p_\perp \sim n$. *Hau et al.* [1993] found using their model that the magnetosheath pressures typically evolve with a dependence which is in between double adiabatic ($\gamma_\perp = 2$ and $\gamma_\parallel = 3$) and isothermal ($\gamma_\perp = \gamma_\parallel = 1$).

4. Summary of Results

We have carried out a 2-D global hybrid simulation to study the structure of the magnetosheath for a case in which the bow shock is a perpendicular shock in the

Table 1. Double Polytropic Indices[a]

θ_0	$\gamma_\perp$	$\gamma_\parallel$
90°	1.07	1.51
60°	1.29	0.58

[a]The values $\gamma_\perp$ and $\gamma_\parallel$ were determined by minimizing the standard deviation in $C_\perp/\langle C_\perp\rangle$ and $C_\parallel/\langle C_\parallel\rangle$, respectively, based on the simulation data.

subsolar region. In particular, the wave activity and the evolution of pressures in the magnetosheath are investigated. Here we summarize the results:

1. Wave activity: In the bow shock transition, the value of $p_\perp/p_\parallel$ increases to a very large value because of the conversion of the large solar wind inflow velocity to a thermal velocity gyrating around the magnetic field. Large-amplitude in-phase oscillations of B and n are seen near the shock transition, indicating the quasi-perpendicular magnetosonic/fast mode; this result is in agreement with observations by *Lacombe et al.* [1992]. Alfvén/ion-cyclotron waves (most likely driven by the anisotropy of the plasma pressure) are observed at all data segments along the streamlines; their power peaks in the middle magnetosheath. The decrease in power toward the magnetopause is consistent with the results of *Hubert* [1994], *Song et al.* [1994], and *Hubert et al.* [1998]. The presence of these waves is evidence that there may be energy exchange from $p_\perp$ to $p_\parallel$ in the simulations. Away from the shock transition, $p_\perp/p_\parallel$ decreases to a moderate value. Antiphase oscillations in B and n are present, and these waves have long wavelengths up to the order of Earth radii (Figure 2). Along flow streamlines, $p_\perp/p_\parallel$ falls to a value near that of *Anderson et al.*'s [1994] formula (3), which represents a condition close to marginal stability for the proton cyclotron wave, and stays near or below that value. The ratio $p_\perp/p_\parallel$ also stays above or near the marginal stability condition of the mirror mode wave.

2. Pressure evolution: Using our 2-D hybrid code simulation of the magnetosheath, we have tested the double adiabatic models and the bounded anisotropy model for the evolution of thermal pressures in the magnetosheath. An attempt has also been made to fit the simulated pressure evolution with the double polytropic model.

3. The double adiabatic model cannot model the physics of the pressure evolution in the magnetosheath.

4. The bounded anisotropy model appears to do a good job of describing the evolution of $p_\perp$, and this is evidence that the kind of energy exchange described by the model is taking place. The evolution of $p_\parallel$ does not appear to be as well described.

5. Our test indicates that the double polytropic model is capable of fitting the pressure evolution very well (not shown). Nevertheless, it must be remembered that the double polytropic model is an empirical fit with several free parameters, $\gamma_\perp$, $\gamma_\parallel$, $\langle C_\perp\rangle$, and $\langle C_\parallel\rangle$. It is difficult to infer the underlying physics from the double polytropic results unless they indicate that the plasma is isothermal or double adiabatic. In addition, the results shown in Table 1 are sensitive to the minimization procedure used. For example, starting with the initial values of pressure and minimizing the deviation of $p_{\perp\mathrm{DP}} - p_\perp$ (as was done for the bounded anisotropy model) led to $\gamma_\perp = 0.61 \neq 1$.

5. Discussion

In the real magnetosheath, enhanced Alfvén/ion-cyclotron wave activity is sometimes observed near the magnetopause where the plasma beta is very low (particularly for northward IMF) [*Anderson et al.*, 1994]. In our hybrid simulation, beta does not become nearly as low as is sometimes observed in the plasma depletion layer, and we also do not observe enhanced Alfvén/ion-cyclotron activity there. (Also note that the streamlines do not get very close to the magnetopause, as can be seen from Figure 1.) Also, while we do have some evidence for the mirror mode in our simulation, in the real magnetosheath the presence of alpha particles (He^{2+}) decreases the growth rate of the proton cyclotron instability (which lead to Alfvén/ion-cyclotron waves) and increases the likelihood that the mirror mode will be observed [*Price et al.*, 1986].

The most likely effect leading to the discrepancy between the bounded anisotropy $p_{\parallel\mathrm{BAM}}$ and $p_\parallel$ from the hybrid simulation is the neglect of the parallel heat flux. We know that this term is not included in the double adiabatic equations [*Chew et al.*, 1956] upon which the bounded anisotropy model is based. The parameter indicating the relative importance of the heat flux is $(\tau_{ms} v_{\parallel th})/L_\parallel$, where $v_{\parallel th}$ is the parallel thermal velocity, $L_\parallel$ is the parallel scale length, and τ_{ms} is the transit time across the magnetosheath.

The parameter $(\tau_{ms} v_{\parallel th})/L_\parallel$ at the two streamlines with $\theta_0 = 90°$ and 60° in the hybrid simulation can be estimated as follows. The convection scale length across the subsolar magnetosheath is $L_\parallel \sim 18\ R_E = 108\lambda_0$. Considering the slow convection speed along the Sun-Earth line and the fact that the flow stagnates in front of the subsolar magnetosphere, the convection time across the subsolar magnetosheath is $\tau_{ms} > 100\Omega_0^{-1}$. The parallel thermal speed $v_{\parallel th} \simeq 1.5 V_{A0}$ on average. Thus

$(\tau_{ms} v_{\|th})/L_{\|} > 1.4$. The fact that this number is greater than unity indicates that the heat conduction plays an important role during the convection. For the 60° streamline, the convection time $\tau_{ms} \simeq 44\Omega_0^{-1}$ for an average convection speed of $3V_{A0}$ across the magnetosheath from the dayside to the flanks, and the average $L_{\|} \simeq 30\ R_E$ in the azimuthal direction. Thus $(\tau_{ms} v_{\|th})/L_{\|} \simeq 0.4$, which also indicates that the heat conduction is not insignificant. Note that in the 3-D situation the convection will not be stopped at the subsolar magnetopause. Our 2-D hybrid simulation may have exaggerated the transient time across the magnetosheath because of the pileup of the plasma in front of the magnetopause boundary. In the real magnetosheath, for a parallel temperature of $\sim 10^6$ K and average convection speed of ~ 150 km s^{-1} across the magnetosheath, the number $(\tau_{ms} v_{\|th})/L_{\|} \simeq 0.6$ on average. This indicates that the heat flux will not be quite as important in the real magnetosheath. (*Denton et al.* [1994] argued that the heat flux could be neglected in the depletion layer.)

Another effect not included by the bounded anisotropy model is time dependence in the ability of waves to regulate the pressure ratio. From Figure 3 we see that $p_\perp/p_\|$ from the hybrid simulation oscillates. This can be understood as the following. Because of the large initial overshoot in the anisotropy ratio $(p_\perp/p_\|)_{\rm Hyb}$ downstream of the bow shock, as shown in Figure 2, a large wave amplitude develops which transfers a large amount of energy from $p_\perp$ to $p_\|$. This reduces $p_\perp/p_\|$, as seen in Figure 2, to the extent that the ion-cyclotron waves are stable. At this point the wave amplitude dies down and possibly transfers some energy back to the ions, but then the compression of field lines that drape around the magnetopause causes the anisotropy to increase. The oscillation timescale would be determined by the timescale for wave growth and damping $\sim 10\Omega_p^{-1}$.

The bounded anisotropy model allows $p_\perp/p_\|$ to vary up to $(p_\perp/p_\|)_{\rm And}$ unimpeded by wave activity; then $p_\perp/p_\|$ is not allowed to exceed $(p_\perp/p_\|)_{\rm And}$. This assumption is best justified if the timescales associated with wave growth and damping, $\sim 10\Omega_p^{-1}$, are small compared to the timescale associated with changes in pressure anisotropy $\sim \tau_{ms}$. In that case we expect some sort of steady state to develop with a constant amount of wave activity. In our hybrid simulation, $\tau_{ms}/(10\Omega_p^{-1}) \sim 13$. For the real magnetosheath we estimate $B \simeq 30$ nT, speed across the magnetosheath $\sim$ 150km s^{-1}, and magnetosheath width $\sim 3\ R_E$, and get $\tau_{ms}/(10\Omega_p^{-1}) \sim 40$, indicating that such time-dependent effects may be less important in the real magnetosheath. These time-dependent effects would be difficult to model; one needs to integrate the growth of the waves over time depending on the instantaneous plasma parameters.

Finally, it is noted that the case shown in this paper is only for the magnetosheath with a perpendicular shock at the subsolar line. The kinetic structure of the magnetosheath is expected to vary if the IMF orientation is different. Further systematic simulations are necessary for the understanding of the presence of various kinetic wave instabilities and their effects on the magnetosphere.

Acknowledgments. This work was supported by NASA grant NAG5-8081 and NSF grant ATM-9805550 to Auburn University, NSF grant ATM-9911975 and NASA grant NAG 5-7442 to Dartmouth College, NSC grant 90-2111-M-008-003 to National Central University, and an NSC grant to National Cheng Kung University. Computer resources were provided by the National Partnership for Advanced Computational Infrastructure, the Arctic Region Supercomputer Center, and the Alabama Supercomputer Center.

Janet G. Luhmann thanks Daniel Hubert and another referee for their assistance in evaluating this paper.

References

Anderson, B. J., S. A. Fuselier, and D. Murr, Electromagnetic ion cyclotron waves observed in the plasma depletion layer, *Geophys. Res. Lett., 18*, 1955, 1991.

Anderson, B. J., S. A. Fuselier, S. P. Gary, and R. E. Denton, Magnetic spectral signatures in the Earth's magnetosheath and plasma depletion layer, *J. Geophys. Res., 99*, 5877, 1994.

Chew, G. F., M. L. Goldberger, and F. E. Low, The Boltzmann equation and the one-fluid hydromagnetic equations in the absence of particle collisions, *Proc. R. Soc. London, Ser. A., 236*, 112, 1956.

Crooker, N. U., and G. L. Siscoe, A mechanism for pressure anisotropy and mirror instability in the dayside magnetosheath, *J. Geophys. Res., 82*, 185, 1977.

Crooker, N. U., T. E. Eastman, and G. S. Stiles, Observation of plasma depletion in the magnetosheath at the dayside magnetopause, *J. Geophys. Res., 84*, 860, 1979.

Denton, R. E., and J. G. Lyon, Density depletion in an anisotropic magnetosheath, *Geophys. Res. Lett., 23*, 2891, 1996.

Denton, R. E., and J. G. Lyon, Effect of pressure anisotropy on the structure of a two-dimensional magnetosheath, *J. Geophys. Res., 105*, 7545, 2000.

Denton, R. E., B. J. Anderson, S. P. Gary, and S. A. Fuselier, Bounded anisotropy fluid model for ion temperatures, *J. Geophys. Res., 99*, 11,225, 1994.

Denton, R. E., S. P. Gary, X. Li, B. J. Anderson, J. W. LaBelle, and M. Lessard, Low-frequency fluctuations in the magnetosheath near the magnetopause, *J. Geophys. Res., 100*, 5665, 1995a.

Denton, R. E., et al., Bounded anisotropy fluid model for ion temperature evolution applied to AMPTE/IRM magnetosheath data, *J. Geophys. Res., 100*, 14,925, 1995b.

Denton, R. E., M. R. Lessard, J. W. LaBelle, and S. P. Gary, Identification of low–frequency magnetosheath waves, *J. Geophys. Res., 103*, 23,661, 1998.

Erkaev, N. V., C. J. Farrugia, and H. K. Biernat, Three-dimensional, one-fluid, ideal MHD model of magnetosheath flow with anisotropic pressure, *J. Geophys. Res., 104*, 6877, 1999.

Fairfield, D. H., Average and unusual locations of the Earth's magnetopause and bow shock, *J. Geophys. Res., 76*, 6700, 1971.

Farris, M. H., C. T. Russell, and M. F. Thomsen, Magnetic structure of the low beta, quasi-perpendicular shock, *J. Geophys. Res., 98*, 15,285, 1993.

Fuselier, S. A., B. J. Anderson, S. P. Gary, and R. E. Denton, Ion anisotropy/beta correlations in the Earth's quasi-parallel magnetosheath, *J. Geophys. Res., 99*, 14,931, 1994.

Gary, S. P., The mirror and ion cyclotron anisotropic instabilities, *J. Geophys. Res., 97*, 8519, 1992.

Gary, S. P., B. J. Anderson, R. E. Denton, S. A. Fuselier, and M.E. McKean, A closure relation for anisotropic plasmas from the Earth's magnetosheath, *Phys. Plasmas, 1*, 1676, 1994.

Gary, S. P., M. E. McKean, and D. Winske, Proton temperature anisotropy in the magnetosheath: Hybrid simulations, *Geophys. Res. Lett., 23*, 2887, 1996.

Hasegawa, A., *Plasma Instabilities and Nonlinear Effects*, Springer-Verlag, New York, 1975.

Hau, L.-N., and B. U. Ö. Sonnerup, On slow-mode waves in an anisotropic plasma, *Geophys. Res. Lett., 20*, 1763, 1993.

Hau, L.-N., et al., Double-polytropic closure in the magnetosheath, *Geophys. Res. Lett., 20*, 2255, 1993.

Hill, P., G. Paschmann, R. A. Treumann, W. Baumjohann, N. Sckopke, and H. Lühr, Plasma and magnetic field behavior across the magnetosheath near local noon, *J. Geophys. Res.*, 100, 9575, 1995.

Hubert, D., Nature and origin of wave modes in the dayside Earth magnetosheath, *Adv. Space Res., 14*(7), 55, 1994.

Hubert, D., C. Perche, C. C. Harvey, C. Lacombe, and C. T. Russell, Observation of mirror waves downstream of a quasi-perpendicular shock, *Geophys. Res. Lett., 16*, 159, 1989.

Hubert, D., C. Lacombe, C. C. Harvey, M. Moncuquet, C. T. Russell, and M. F. Thomsen, Nature, properties, and origin of low-frequency waves from an oblique shock to the inner magnetosheath, *J. Geophys. Res., 103*, 26,783, 1998.

Johnson, J. R., and C. Z. Cheng, Global structure of mirror modes in the magnetosheath, *J. Geophys. Res., 102*, 7179, 1997.

Kaufmann, R. L., J.-T. Horng, and A. Wolfe, Large amplitude hydromagnetic waves in the inner magnetosheath, *J. Geophys. Res., 75*, 4666, 1970.

Krauss-Varban, D., N. Omidi, and K. B. Quest, Mode properties of low-frequency waves: Kinetic theory versus Hall-MHD, *J. Geophys. Res., 99*, 5987, 1994.

Lacombe, C., F. G. E. Pantellini, D. Hubert, C. C. Harvey, A. Mangeney, G. Belmont, and C. T. Russell, Mirror and Alfvénic waves observed by ISEE-2 during crossings of the Earth's bow shock, *Ann. Geophys., 10*, 772, 1992.

Lee, L. C., C. P. Price, C. S. Wu, and M. E. Mandt, A study of mirror waves generated downstream of a quasi-perpendicular shock, *J. Geophys. Res., 93*, 247, 1988.

Lees, L., Interaction between the solar wind and the geomagnetic cavity, *AIAA J., 2*, 1576, 1964.

Lin, C.-H., J. K. Chao, L. C. Lee, D. J. Wu, Y. Li, and B. H. Wu, Identification of mirror waves by the phase difference between perturbed magnetic field and plasmas, *J. Geophys. Res., 103*, 6621, 1998.

Lin, Y., D. W. Swift, and L. C. Lee, Simulation of pressure pulses in the bow shock and magnetosheath driven by variations in interplanetary magnetic field direction, *J. Geophys. Res., 101*, 27,251, 1996.

McKean, M. E., D. Winske, and S. P. Gary, Kinetic properties of mirror waves in magnetosheath plasmas, *Geophys. Res. Lett., 19*, 1331, 1992.

Midgely, J. E., and L. Davis Jr., Calculation by a moment technique of the perturbation of the geomagnetic field by the solar wind, *J. Geophys. Res., 68*, 5111, 1963.

Paschmann, G., N. Sckopke, and G. Haerendel, ISEE plasma observations near subsolar magnetopause, *Space Sci. Rev., 22*, 717, 1978.

Phan, T.D., G. Paschmann, W. Baumjohann, N. Sckopke, and H. Lühr, The magnetosheath region adjacent to the dayside magnetopause: AMPTE/IRM observations, *J. Geophys. Res., 99*, 121, 1994.

Price, C. P., D. W. Swift, and L. C. Lee, Numerical simulation of nonoscillatory mirror waves at the Earth's magnetosheath, *J. Geophys. Res., 91*, 101, 1986.

Pudovkin, M. I., B. P. Besser, V. V. Lebedeva, S. A. Zaitseva, and C.-V. Meister, Magnetosheath model in the Chew-Goldberger-Low approximation, *Phys. Plasmas, 6*, 2887, 1999.

Samsonov, A. A., and M. I. Pudovkin, Application of the bounded anisotropy model for the dayside magnetosheath, *J. Geophys. Res., 105*, 12,859, 2000.

Sckopke, N., G. Paschmann, S. J. Bame, J. T. Gosling, and C. T. Russell, Evolution of ion distributions across the nearly perpendicular bow shock: Specularly and nonspecularly reflected gyrating ions, *J. Geophys. Res., 88*, 6121, 1983.

Sckopke, N., G. Paschmann, A. L. Brinca, C. W. Carlson, and H. Luhr, Ion thermalization in quasi-perpendicular shocks involving reflected ions, *J. Geophys. Res., 95*, 6337, 1990.

Song, P., C. T. Russell, and S. P. Gary, Identification of low-frequency fluctuations in the terrestrial magnetosheath, *J. Geophys. Res., 99*, 6011, 1994.

Tsurutani, B. T., E. J. Smith, R. R. Anderson, K. W. Ogilvie, J. D. Scudder, D. N. Baker, and S. J. Bame, Lion roars and nonoscillatory drift mirror waves in the magnetosheath, *J. Geophys. Res., 87*, 6060, 1982.

Winske, D., and K. B. Quest, Magnetic field and density fluctuations at the perpendicular supercritical collisionless shocks, *J. Geophys. Res., 93*, 9681, 1988.

Zwan, B. J., and R. A. Wolf, Depletion of solar wind plasma near a planetary boundary, *J. Geophys. Res., 81*, 1636, 1976.

J. K. Chao, Institute of Space Science, National Central University, Chungli, 32001 Taiwan.

R. E. Denton, Physics and Astronomy Dept., Dartmouth College, Hanover, NH 03755.

L. C. Lee, Physics Dept., National Cheng Kung University, Tainan, 701 Taiwan.

Y. Lin, Physics Dept., Auburn University, Auburn, AL 36849. (ylin@physics.auburn.edu)

(Received June 13, 2000; revised December 18, 2000; accepted December 20, 2000.)